On the radial variation of the transverse mechanical properties of bamboo

On the radial variation of the transverse mechanical properties of bamboo

Luisa Molari[1],

Jose J. García[2]

[1]DICAM, Alma Mater Studiorum Università di Bologna, Bologna, Italy

[2]Escuela de Ingeniería Civil y Geomática, Universidad del Valle, Cali, Colombia

jose.garcia@gmail.com, luisa.molari@unibo.it

ABSTRACT

Bamboo is a functionally graded and axially reinforced material displaying high longitudinal mechanical properties. However, it is prone to longitudinal splitting, mainly due to tensile and shear stress components. Therefore, this experimental study was focused at determining the transverse mechanical properties of five species of bamboo using digital image correlation (DIC). Thus, two tests with parts of rings were used to independently determine the inner and outer circumferential tensile strength as well as the variation of the circumferential Young's modulus through the culm wall. In the first set-up, a semi-ring (SR test) was radially loaded at the middle section and supported on rollers at both ends such that the inner surface of the specimen was under tensile stress. In the second protocol, a specimen bigger than a semi-ring (C test) was loaded by two radially applied compression loads to generate tensile circumferential stresses on the outer surface. A closed-form solution assuming a linear variation of the Young´s modulus through the culm wall was developed to analyze the experimental results. The bamboo species *Phyllostachys edulis* (EDU), *Phyllostachys bambusoides* (BAM), *Phyllostachys Iridescens* (IRI), *Phyllostachys Violascens* (VIO) grown in North of Italy, and *Guadua angustifolia* (GA) grown in Colombia were tested. The inner tensile failure strain (range of means for all species: 0.014-0.035) was generally higher than the outer (range of means for all species: 0.008-0.0019). The effective modulus of GA (931 MPa-1148 MPa) was lower than those of the European species (range of means for all European species: 1209-2983 MPa). The inner Young's moduli for all species except EDU (796-1694 MPa) was lower than the outer (range of means for all species: 1976-4694 MPa). The trend was different for EDU that showed an outer Young's modulus about 30% lower than

the inner modulus. The outer tensile strength of BAM, IRI and GA (range of means for the three species:16.5-30.5 MPa) was significantly higher than the inner (range of means for three species: 9.9-17.6 MPa), while no signficant differences were found for VIO. A different trend was obtained for EDU, for which the inner strength was about three times higher than the outer.

KEYWORDS: *Bamboo, circumferential strength, circumferential Young modulus, functionally graded material, mechanical characterization.*

1.INTRODUCTION

The current devastation of tropical forest and the increased alarms due to global warming have created the need to use sustainable practices in all human activities, such as promulgated by the United Nations in the Sustainable Development Goals [1]. Conventional construction materials like concrete and steel are excellent from the mechanical point-of-view, however, their production is energy intensive. Hence, there is a worldwide search for sustainable construction materials to supply the need to build infrastructure and housing for our current and future generations. Due to its excellent strength in the axial direction, bamboo has become a sustainable alternative to replace traditional materials in many applications [2,3].

First, bamboo is a plant of rapid grow that can be used in construction at 4-6 years of age. Bamboo plantations are a key factor to control water cycles and reduce erosion [4]. It is estimated that a hectare of bamboo *Guadua* can produce 50 m^3 of bamboo a year, compared with 2.3-10 m^3/year for wood [2]. Nowadays, in various countries such as the Europeans, bamboo is not yet considered as a material useful for structural applications. On the other hand, in the Latin-American countries, most of the population perceives bamboo to be a second-quality material only apt for temporary applications. This is due in part to inadequate practices during material handling, construction and maintenance. Though important advances have been made to regulate the use of the material [5], many technical challenges remain before bamboo can be fully accepted as an engineering material.

Bamboo culms are cylindrical tubes reinforced with transverse diaphragms located at variable distances along the length. Bamboo culms are functionally graded and axially reinforced with strong cellulose fibers. Therefore, the material displays excellent mechanical properties along the axial direction of the culm but it is prone to longitudinal splitting on the fiber planes [6]. This failure mode becomes critical close to the zones of stress concentrations, such as the through holes used in traditional joints. Thus, the structural bamboo elements usually fail by longitudinal splitting at axial stress levels one order of magnitude lower than the axial strength. Longitudinal splitting has been attributed to the low tensile circumferential strength [7,8].

Various experimental set-ups [8-13] have been proposed to determine the transverse mechanical properties of bamboo, which depend on the radial position.

Torres et al [10] proposed the diametric compression test of bamboo rings that is now included in the 22175 ISO standard [5]. The test allows estimating the effective circumferential elastic modulus and the apparent bending strength perpendicular to the fibers. The splitting test, also included in the 22175 ISO standard, allows estimating the tension strength perpendicular to the fibers. Whereas the geometry of the splitting test is relatively involved, the diametric compression test, also called the edge bearing test, is simple but the failure initiates either on the outer or inner surface of the ring. Another simple test consists of loading parts of bamboo rings perpendicular to its flat surface, inducing torsion and bending [11], which allowed measuring the radial-circumferential Poisson ratio, the circumferential Young modulus and the circumferential-longitudinal shear modulus of *Guadua angustifolia* [14].

Efforts have also been made to measure the variation of the transverse properties along the culm wall. To determine the variation of circumferential properties along the wall thickness, Sharma et al. [8] carry out the edge bearing test with concentric annular sections. However, the experimental procedure is not simple, and the authors indicate that more research is needed to elucidate the radial variation of the transverse properties. Lee et al. [9] loaded bamboo rings under internal pressure to analyze the variation of the circumferential modulus through the culm wall by fitting linear, power, and exponential distributions to the inner and outer strain measurements. Unfortunately, Lee et al. [9] did not report the species used. A different set up is the so called flat-ring test, where a flat ring is loaded in a sort of four-point bending test [12]. The flat-ring test [15] was used recently to estimate the variation of bamboo elastic properties using measured volumes of the constituents, however no validation of the estimated properties was accomplished.

Using the edge-bearing test, the graded variation of the circumferential modulus was obtained using digital image correlation (DIC) measurement of the strain field and a relatively complex minimization process using finite element models [13]. In this test, the ring is under bending moment that changes sign with the position along the ring circumference. Hence, the ring may fail at the inner or at the outer location of the wall thickness, which does not allow to independently determine the inner and outer circumferential tensile strength.

The objective of this study was to assess the radial variation of the circumferential mechanical properties of five species of bamboo. The bamboo *Phyllostachys* species *Phyllostachys edulis* (EDU), *Phyllostachys bambusoides* (BAM), *Phyllostachys Iridescens* (IRI), *Phyllostachys Violascens* (VIO) grown in the North of Italy (identified here as European species) and *Guadua angustifolia* (GA) grown in Colombia were tested. We used two simple tests with parts of rings that allow the independent determination of both [16], the inner and the outer circumferential strength of the material, using the strain fields measured with DIC. The experimental study was complemented with the derivation of a closed-form formula to find the inner and outer elasticity moduli. This information may be used for a more reliable prediction of longitudinal splitting using

theoretical finite element models or for the mechanical assessment of laminated bamboo products.

2. Materials and Methods

2.1 Material

The specimens of the European bamboo were not immunized or oven dried. On the other hand, the specimens of *Guadua angustifolia* (GA) were borax treated and oven dried with practices well established [3]. Moisture is reported in Table 1 whereas the dimensions of the specimens are summarized in Figure 1. The diameter and thickness of GA is about 1.5 and 2 times higher than the respective diameter and thickness of the European species. For all the species, the rings can be considered thin since the relation of diameter to thickness is around 10. The specimens were cut at a nominal width of 20 mm.

Table 1. Moisture content of the tested specimens and the coefficient of variation COV within parenthesis

	BAM (n=12)	EDU (n=12)	IRI(n=12)	VIO (n=12)	GA (n=24)
Mean water content	9.59	9.09	9.11	8.93	11.60
COV	(0.08)	(0.03)	(0.04)	(0.02)	(0.04)

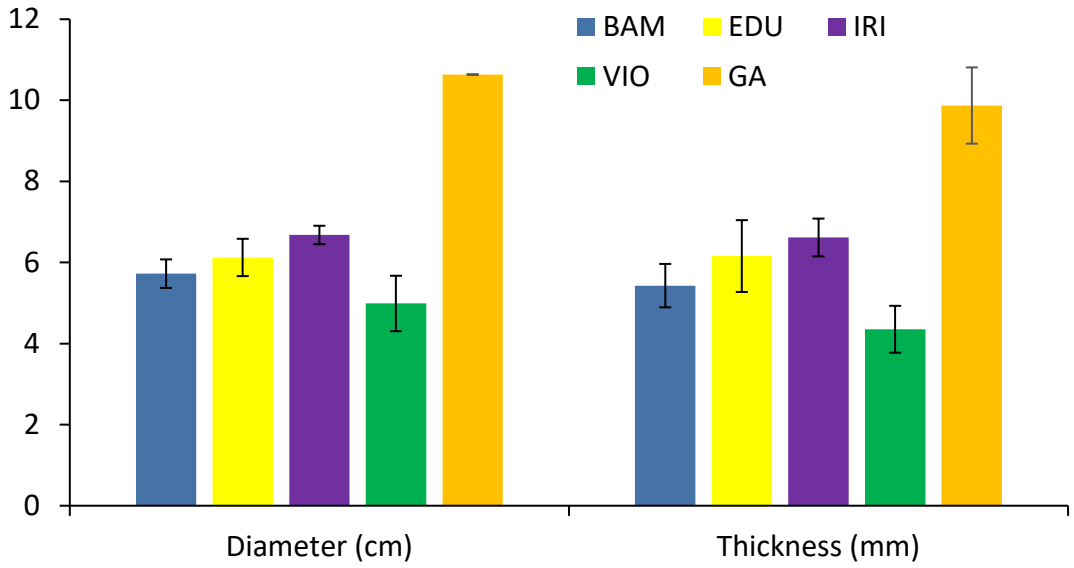

Figure 1. Summary of diameter (cm) and thickness (mm) of the specimens (n = 12 for the European species and n =24 for GA). The error bars represent the standard deviation

2.2. Experimental methods

Two experimental set-ups were used [16] to characterize the circumferential behavior of bamboo. In the first set up, the semi-ring (SR) test represented in Figure 2.a, bamboo

semi-rings are radially loaded at the middle section and supported at the ends using small steel plates resting on solid cylinders to avoid horizontal reactions. The moment at the center of the semi-ring can be calculated as the vertical reaction (half of the applied force) times the internal radius of the semi-ring as validated with FE model in the following section. The load tries to open the semi-ring and the inner surface of the wall is exposed to circumferential tensile stress.
In the second set-up (Figure 2b), we used portions bigger than a semi-ring with a shape like the letter C (C test) to facilitate the test. The specimens were obtained by removing an arc of about 90°. These samples were then subjected to two radially opposed compression loads. In this case, the load closes the specimen and the circumferential tensile stresses occur on the outer surface of the wall.

The specimens were tested in the LISG Laboratory at the University of Bologna, Italy. The load was applied using a universal hydraulic press, WOLPERT, while two STINGRAY cameras were used to perform digital image correlation (DIC) to measure the strain field at the zone of interest (Figure 3). For the DIC measurements, the zone of interest was carefully sanded with abrasive paper to ensure a smooth surface for the first layer of RAL 9010 matt white spray paint. Next, three to four layers of the white spray paint were successively applied to generate a consistent ground coat. Finally, to produce a random speckle pattern over the white varnish, a FOLIATEC spray film was applied. The software VIC 3D 2012 (Correlated Solutions, Ltd.) was used to track the speckle pattern to calculate the strain contours.

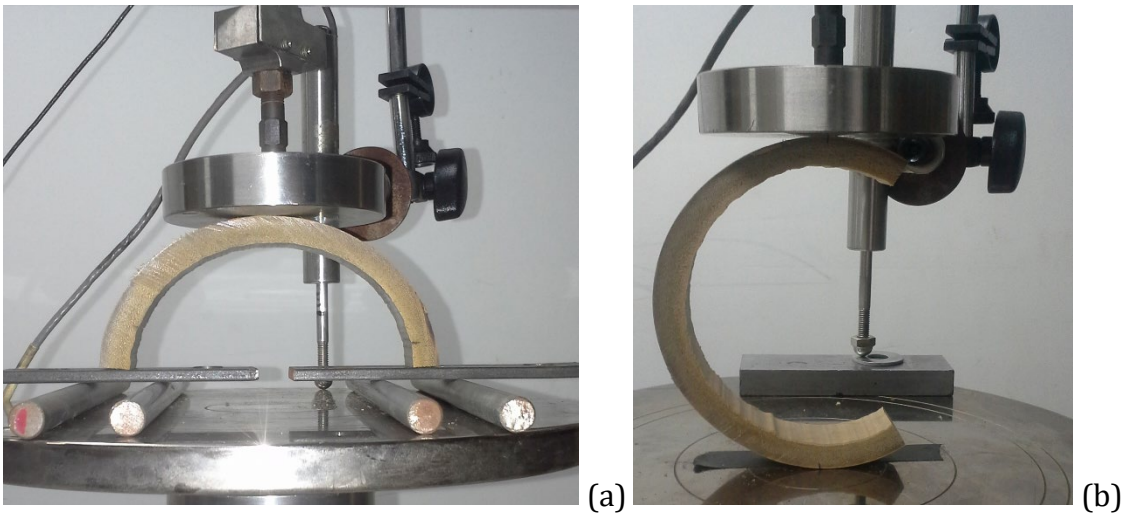
(a) (b)

Figure 2. Used set-ups: a. SR test, b. C test.

Displacement control was used in all the cases at a speed of 1 mm/min for the first configuration and 2 mm/min for the second. A higher velocity for the second configuration was used since this set-up is more compliant than the first.
For each of the European species, twelve specimens were cut from three culms, six from the lower part (between 0.5 and 1.5 from the ground) and six from the higher (between

2.5 and 3.5 m from the ground) part of the culms. Six were used for the SR test and six for the C test. In the case of the C test for BAM six specimens were tested but only the data of two specimens were recovered with DIC due to failures of the data acquisition program. For GA, 12 specimens were used for the SR test and 12 for the C test, however, no differentiation could be made about the position in the culm.

Figure 3. The set up for the semi-ring test with DIC

2.3. Analytical Model

A closed-form solution was obtained assuming a curved beam with a linear variation of the circumferential elastic modulus along the thickness. The formula for a homogeneous material (i.e. elastic modulus constant with radial position) is presented in various books [17]. For the sake of brevity, only the main results are described below. The procedure to derive the closed-form solution is included as supplementary material. For a curved beam, the neutral axis does not coincide with the centroid. Hence, the results are presented in terms of the distance *e* from the centroid to the neutral axis, positive toward the center of curvature (Figure 4).

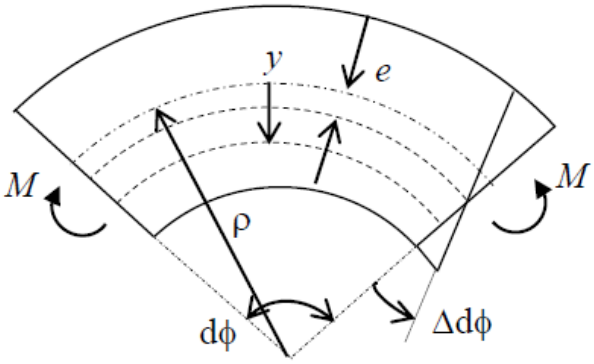

Figure 4. Infinitesimal element of a curved beam under a bending moment M. Plane sections are assumed to remain plane. $\Delta d\varphi$ is the rotation angle of the right cross section with respect to the left, while e is the distance from the centroid to the neutral axis.

Considering a constant Young modulus, the normal stress σ and the distance e can be calculated as,

$$\sigma = \frac{M\,(y-e)}{mA(\rho-e)(\rho-y)}, \tag{1}$$

$$e = \frac{m\left(1-\frac{\rho N}{M}\right)}{\frac{1+m}{\rho}-\frac{mN}{M}}, \tag{2}$$

where N is the normal force, M is the bending moment, ρ is the radius of the centroidal axis, A is the area of the cross section, and y is the radial coordinate measured from the centroidal axis (Figure 4). The parameter m can be calculated with the following equation,

$$m = \frac{\rho}{t}\ln\left(\frac{R_o}{R_i}\right) - 1 \tag{3}$$

where R_o and R_i are the outer and inner radii of the ring, and t is the thickness of the specimen.

For the semi-ring, the normal force is zero, and the moment is equal to half of the applied force times the radius. In the C test the compression normal force is equal to the applied force, and the moment is equal to the force times the radius.

Next, bamboo was represented as a graded material with a Young modulus varying linearly along the thickness as described by:

$$E = c_0 + c_1(\rho - y), \tag{4}$$

where c_0 and c_1 are two constant parameters that can be related to the inner (E_i) and outer (E_o) moduli as,

$$c_0 = E_i - \left(\frac{R_i}{t}\right)(E_o - E_i) \tag{5}$$

$$c_1 = \frac{E_o - E_i}{t}. \tag{6}$$

For this case, the theoretical analysis showed that σ and e can be calculated with the following formulas:

$$\sigma = \frac{M\left[1+\left(\frac{c_1}{c_0}\right)(\rho-y)\right](y-e)}{\left[(\rho-e)mA+\left(\frac{c_1}{c_0}\right)I\right](\rho-y)}, \tag{7}$$

$$e = \frac{\frac{N}{M}(c_0\rho mA+c_1 I)-c_0 mA}{\frac{N}{M(c_0 mA)}-c_0\frac{A}{\rho}(1+m)-c_1 A}. \tag{8}$$

Further details are reported in Appendix A.

A quadratic distribution for the circumferential modulus was also considered. However, for the typical material properties presented by Moran et al. [13], the stress distribution under linear and quadratic variation of the elastic modulus were substantially similar. Hence, for the sake of simplicity, only the linear graded model was used.

2.4.Procedure to calculate circumferential strength and Young moduli

The effective modulus was calculated by fitting a straight line to the force-deflection curve between 20% and 60% of the maximum load. Next, with the slopes *S* of the lines, the effective moduli were calculated with the following formulas:

$$E_f = \frac{6(3\pi/4-2){R_i}^3}{bt^3}\,\mathrm{S}, \tag{9}$$

for the semi-ring,

$$E_f = \frac{6\pi\rho^3}{bt^3}S, \tag{10}$$

for the C shape. The formulas can be obtained using the Castigliano's theorem as described in Appendix B.

For the linear varying formulation, the stresses σ_o and σ_i at the outer and at inner positions of the middle cross section can be obtained in terms of E_i and E_o with equations (4)-(8). Next, the inner and the outer moduli were obtained by solving the following two non-linear algebraic equations:

$$\begin{cases}\sigma_o(E_i, E_o) = E_i\,\varepsilon_o \\ \sigma_i(E_i, E_o) = E_o\,\varepsilon_i\end{cases} \tag{11}$$

where ε_o and ε_i were acquired with DIC. Again, for this case, the moduli were calculated with the slope between 20% and 60% of the peak load, as suggested by the standard for the tensile test.

The reported strength is the maximum tensile stress at the failure load calculated with the aforementioned equations. ANOVA statistical analysis was accomplished to stabish significant differences. Significant differences were accepted if p was lower than 0.05.

2.5.Finite element verification of the closed-form solution

A finite element model was developed with the commercial program ABAQUS to verify the procedure to determine the graded elastic moduli using the semi-ring test (Figure 5). A contact model was adopted, which considers the variation of the line of contact between the semi-ring and the lower supports, due to rotations of the lower cross sections. Surface-to-surface contacts were defined on the interfaces of the semi-ring with both, the lower supports and the rigid body. As the lower supports of the semi-ring are in contact with separate plates resting on rollers, the contact at the lower supports were defined as friction-free. For the contact with the upper rigid body, a friction coefficient of 0.3 was defined, which is representative of the friction coefficient between wood and steel. A 20 mm wide semi-ring was considered, with inner and outer radii of 45 mm and 55 mm, respectively, which are representative of the dimensions of culms of the *Guadua angustifolia* species.

The axis 1, 2 and 3 were oriented along the radial, circumferential and axial directions, respectively. A transversely isotropic and functionally graded material was defined for the semi-ring, with E_1 and E_2 varying linearly from 686 MPa at the inner edge, to 1611 MPa at the outer edge. To account for the variation of the material properties through the culm wall thickness, an artificial radial temperature field was prescribed, and E_1 and E_2 were defined to be a function of this field [13]. The shear modulus in the plane 1-2 of isotropy was then calculated from the circumferential modulus according to $G_{12} = \frac{E_1}{2(1+\nu_{12})}$, where ν_{12} is the Poisson's ratio on the 1-2 plane, assumed to be 0.22 [12]. The other material properties were assumed to be constant with position as, E_3=12000 MPa, $G_{13} = G_{23} = 800$ MPa, $\nu_{13} = \nu_{23} = 0.01$.

Non-linear geometric effects were included in the analysis. The semi-ring mesh consisted of 7800 eight-node bricks with incompatible modes. A vertical displacement of 1 mm was applied to the upper rigid body.

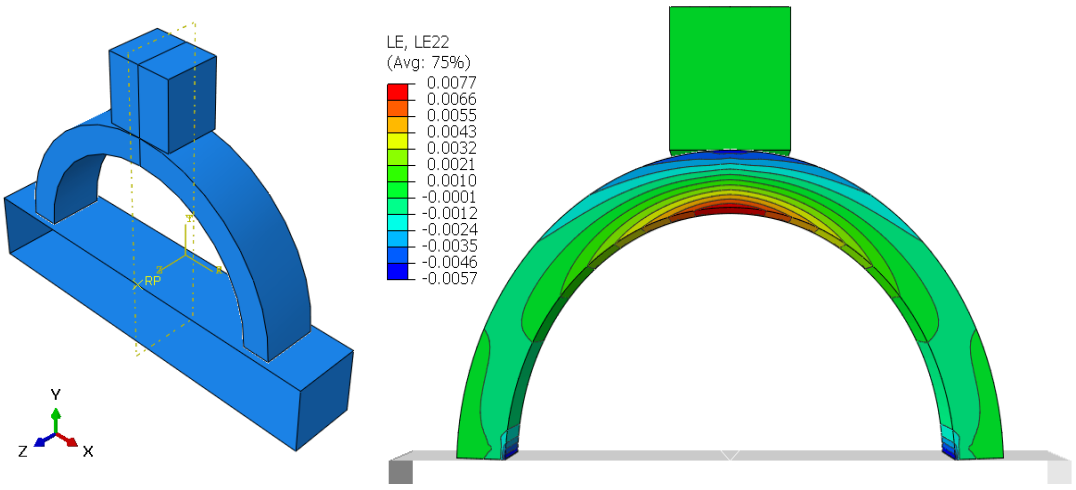

Figure 5. Finite element model (left) and strain distribution (right) for a vertical displacement of 1 mm applied to the upper rigid body

The strain contours (Figure 5) show maximum tensile strains 35% higher than the maximum compressive. When calculating the moment at the middle cross section with the radius of the centroid (ρ), the recovered (as described in 2.4) inner and outer moduli were 728 MPa and 1802 MPa, respectively, which show differences of 6.1% and 11.9% with respect to the FE target value. When the moment was calculated with the inner radius (R_i), the differences were -4.4% and 0.68% compared to the target values (as shown in Figure 6). This procedure is consistent with the observed deformation of the semi-ring that shows contact at the inner line due to the rotation of the lower cross sections.

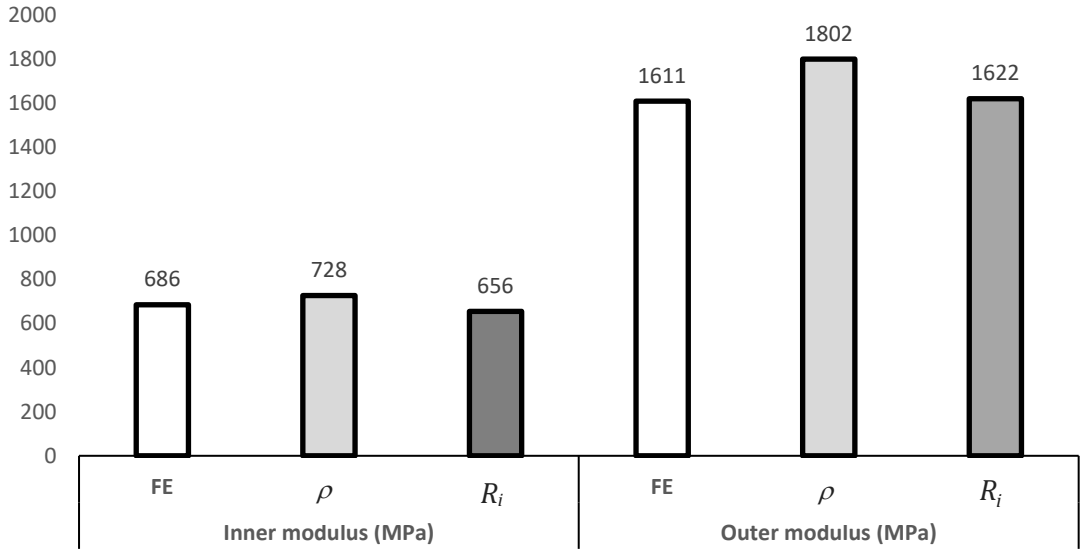

Figure 6. Comparison of the elastic moduli recovered with the analytical solution using the mean radius (ρ) and the inner radius (R_i).

3. RESULTS

3.1 Load displacement curves

Load-displacement curves show an initial straight line followed by a short curve with decaying slope and sudden fracture at the maximum load, which is typical of brittle materials (Figure 7).

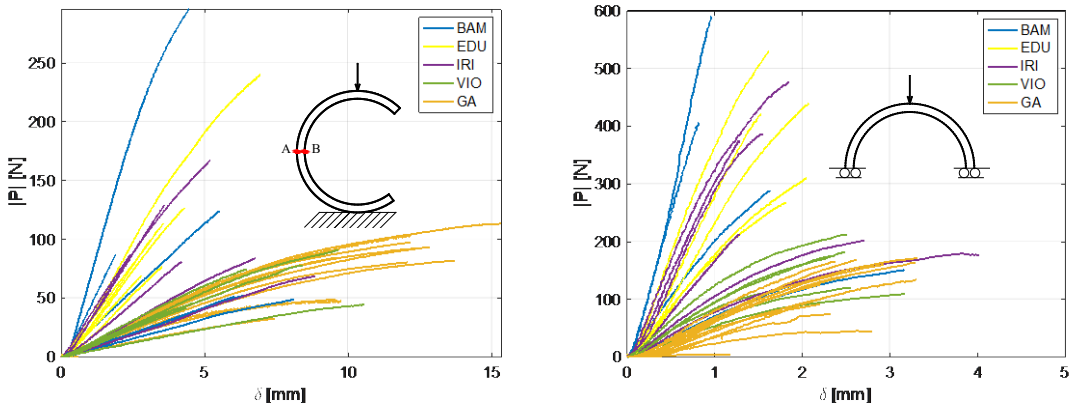

Figure 7. Load displacement curves for the C-shaped (left) and semi-ring tests (right)

For the European species, a lower stiffness was obtained for the specimens from the higher part of the culm compared to the specimens from the lower part, as shown in Figure 8.

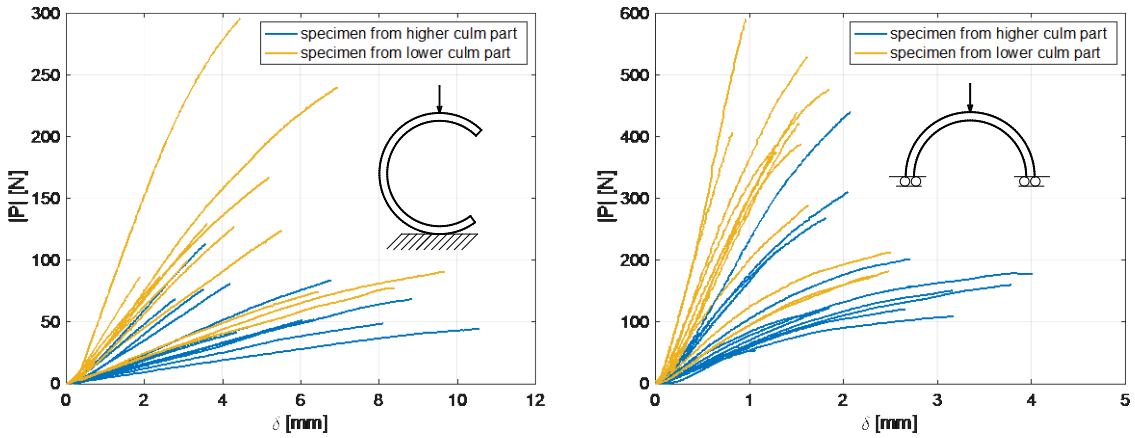

Figure 8. Load displacement curves for the European specimens differentiated by the position in the culm

3.2. Strain distributions

The map of strain can be recovered during the test as represented in Figure 6 for the C-shaped and for the semiring tests, respectively. For the C specimen, the highest tensile strain is located at the most outer part of the middle cross section. For the semi-ring, the peak tensile strain occurs at the inner point of the cross section under the line of force application.

As observed in Figures 9-10, blurry layers formed near the surface that prevented, in some cases, the measurement of strains with DIC. Thus, the maximum values of strain

were recovered using the assumption that plane sections remain plain, which leads to the following formula for strain,

$$\varepsilon = k\frac{(y-e)}{(\rho-y)}, \tag{12}$$

where k is a constant. Thus, two values of strain that could be clearly determined (not located at the surface) were used to calculate both, k and e. Next, maximum strains at the surface were recovered using the appropriate coordinate y. The assumption that plane sections remain plane after deformation was verified using a finite element model.

The graph of the maximum tensile strains on the inner and the outer surfaces (Figure 11 (a)-(c)) versus the load is reported for GA (GAC8), BAM (BAM10B) and EDU (EDU7B). These three cases represent the behaviour of all the specimens. In the first case, the behaviour of GA is non linear in tension and compression. In the second case, representing the behavior of all European species, except EDU, the behaviour is rather linear both in tension and compression. In these two cases the compressive strains are higher than the tensile. For the species Edulis described in the third case, the behaviour is non linear and rather symmetric for positive and negative strains.

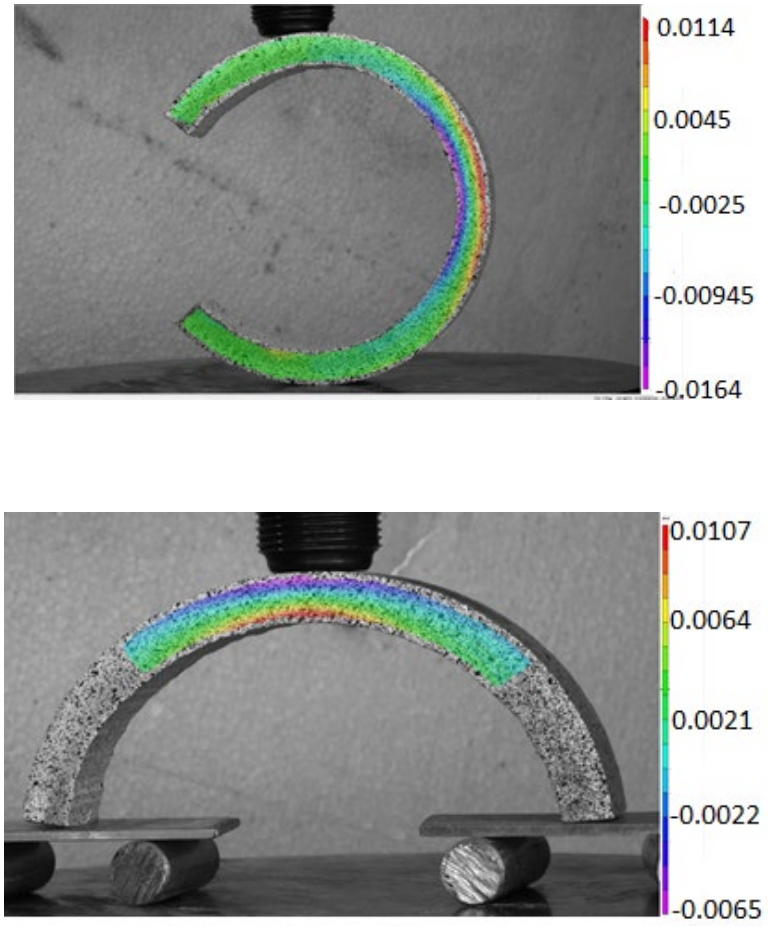

Figure 9. Strain map obtain by Digital Image Corelation: (a) for a C- shaped specimen (GAC1) , (b) for the semiring specimens (GAS22)

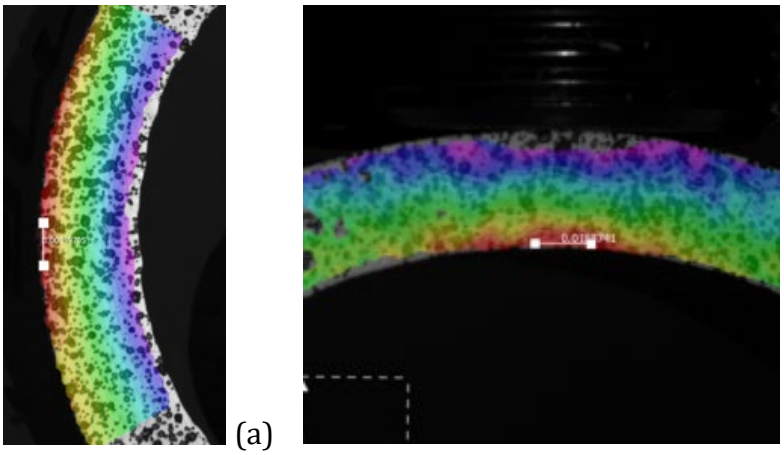

(a) (b)

Figure 10. Extensometer tool used to measure (a) the outer (C-shaped specimen) and (b) the inner (semiring specimen) strain

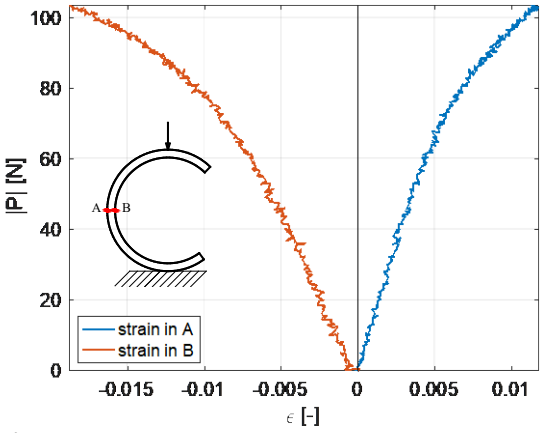

(a)

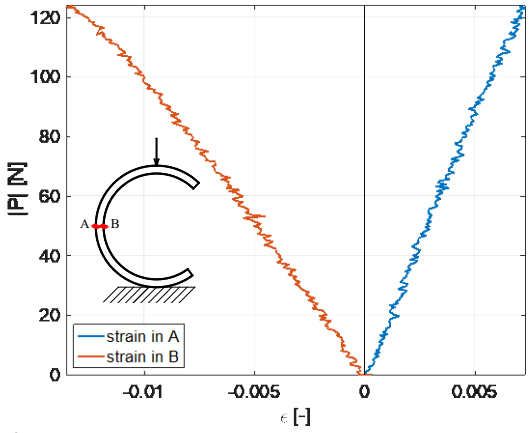

(b)

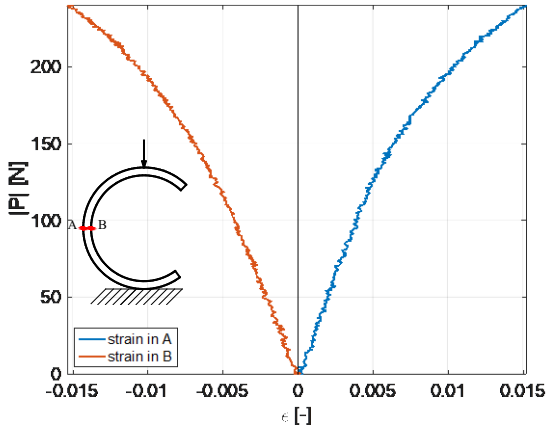

(c)

Figure 11. Load versus strain at the inner and outer points of the cross section where the failure always occurred: (a) Guadua Angustifolia C8 specimen, (b) BAM11B, (c) EDU7B.

The inner failure strains were about 2-3 times significantly higher than the outer failure strains for IRI and VIO, while no significant differences were found for the other species (Figure 12).

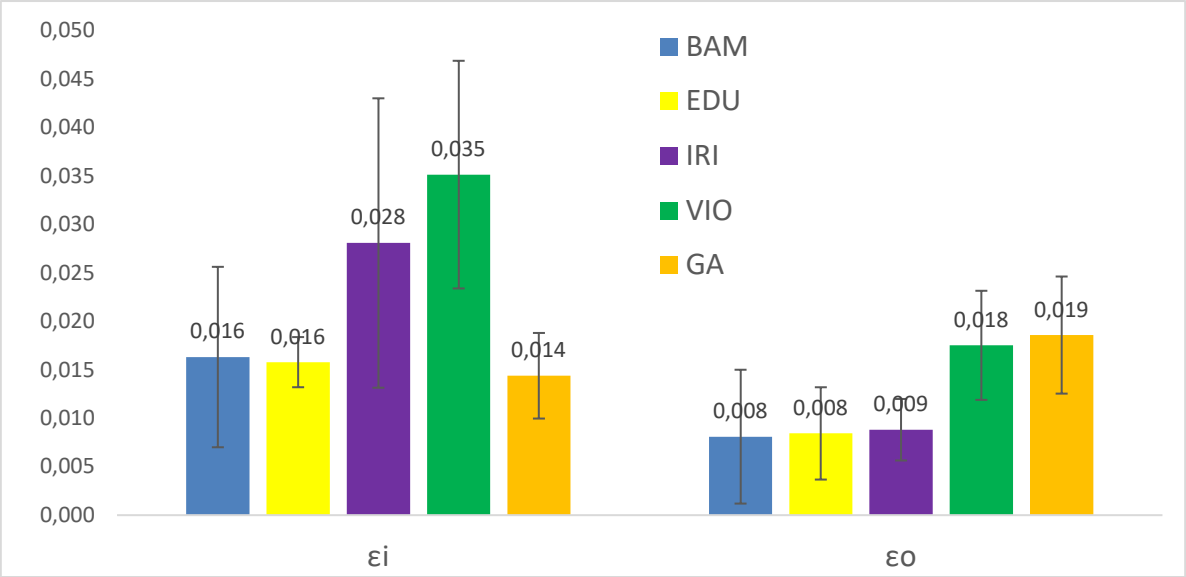

Figure 12. Inner (ε_i) and outer failure (ε_o) strains obtained with the semi-ring and C tests, respectively. The error bars indicate the standard deviation.

3.3 Young modulus

The two different experimental set-ups give occasion to compare the stiffness and tensile strength for both the internal and external culm wall, as the rupture initiated at the tensile sides for the two types of specimens.

For the semi-ring test, the effective Young's modulus of GA was significantly lower than those of the European species. For the C test, the effective Young's modulus of IRI was significantly higher than those of the other species (Figure 13, Table 2). The effective modulus was generally between the inner and the outer for all the species.

The inner and outer Young's moduli showed no difference with respect to the SR and C tests, except for a significant difference for the inner modulus of VIO (Figure 13, Table 2). The outer elastic modulus for BAM and IRI were about 2-3 times higher than the inner moduli in both tests. For VIO and GA the outer modulus was about 1.3-1.8 times significantly higher than the inner in the C tests. The trend is different for Edulis that showed an outer Young's modulus about 30% lower than the inner modulus.

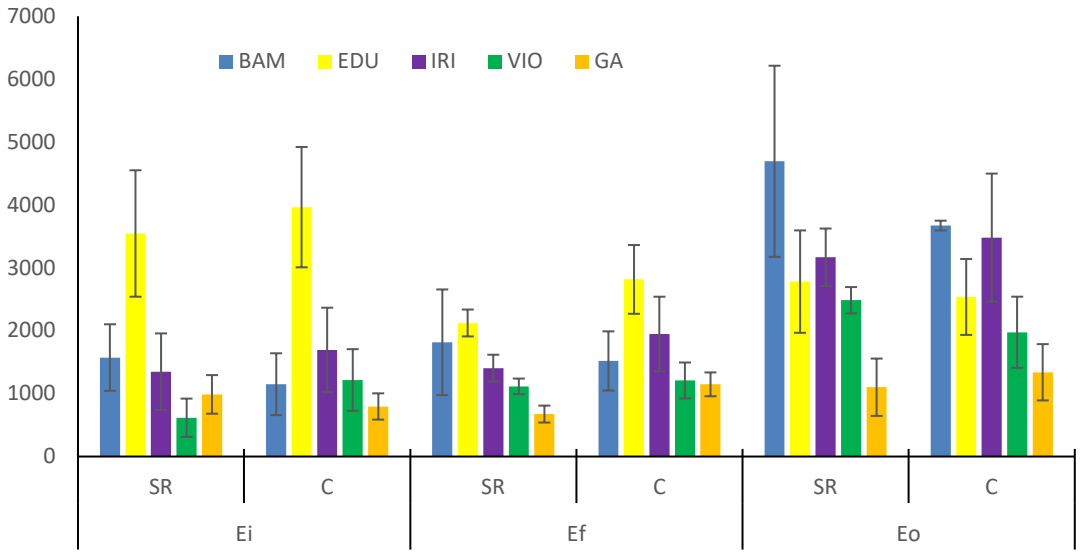

Figure 13. Inner, effective and outer Young's moduli obtained with SR and C tests. The error bars indicate standard deviation.

Table 2. Effective, outer and inner moduli from the SR and C tests. The coefficient of variation is shown within parenthesis, n=6 for the European species and n=12 for GA

	Young Modulus (MPa)					
	E_f		E_i		E_o	
	SR	C	SR	C	SR	C
BAM	2565 (0,51)	1520 (0,31)	1574 (0,34)	1150*(0,43)	4694 (0,32)	3672* (0,02)
EDU	2004 (0,21)	2816 (0,19)	3546 (0,28)	3965(0,24)	2781 (0,29)	2537(0,24)
IRI	2983 (0,07)	1948 (0,30)	1349 (0,45)	1694 (0,40)	3167 (0,14)	3480 (0,29)
VIO	1486 (0,12)	1209 (0,24)	986 (0,96)	1216 **(0,40)	2071 (0,50)	1976 **(0,29)
GA	931 (0,20)	1148 (0,17)	988 (0,31)	796 (0,26)	1102 (0,41)	1340 (0,33)

*in this case the considered specimens are 2, **in this case the considered specimens are 5.

3.4 Circunferential Tensile Strength

The outer tensile strength of BAM, IRI and GA was significantly higher than the inner, while no signficant differences were found for VIO. A different trend was obtained for EDU, for which the inner strength was about three times higher than the outer (Figure 14, Table 3).

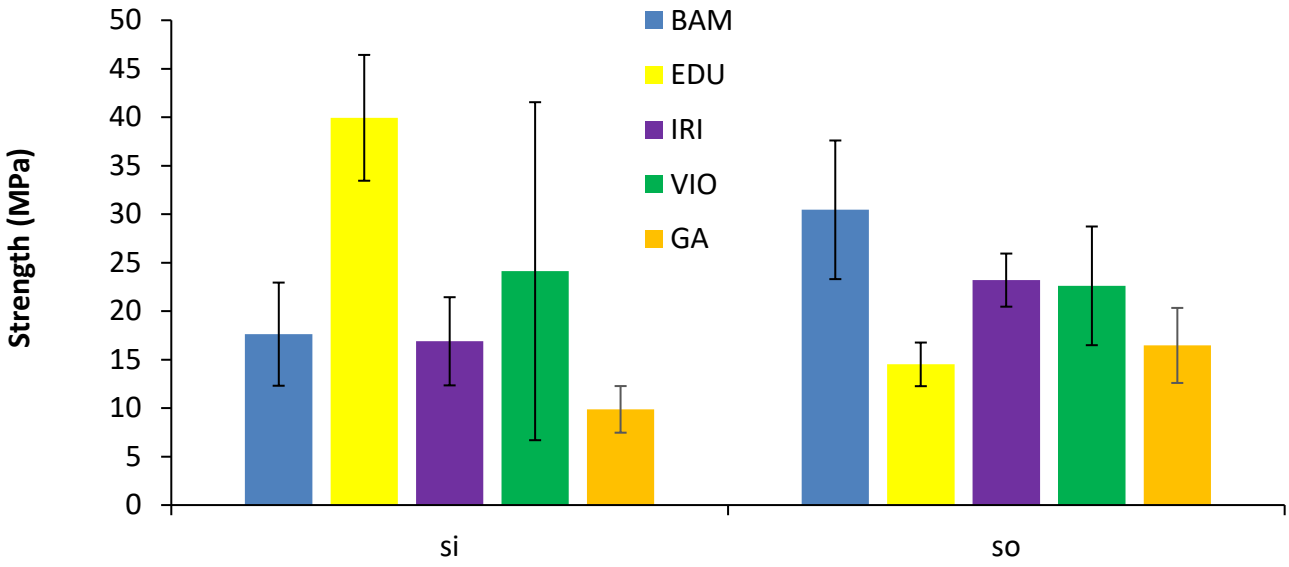

Figure 14. Inner and outer strength obtained with the SR and C tests, respectively. The error bars indicate one standard deviation

Table 3. Summary of the circumferential tensile strength (MPa), the coefficient of variation is in parenthesis.

	Tensile strength (MPa)	
Species	Inner	Outer
BAM	17,6 (0,30)	30,5 (0,23)
EDU	39,9 (0,16)	14,5 (0,16)
IRI	16,9 (0,27)	23,2 (0,12)
VIO	24,1 (0,72)	22,6 (0,27)
GA	9,9 (0,24)	16,5 (0,24)

3.5. Discussion

This study showed differences in the transverse behavior of bamboo, both, with species and with the position through the culm wall. The SR and C tests allowed to independently assess the inner and the outer failure characteristics of the material. Using the strain contours measured with DIC, the outer and inner Young's moduli were estimated with a developed closed-form solution using an algebraic procedure substantially simpler than a finite element minimization scheme accomplished in a previous study [13].

The proposed SR and C tests are compression based and can be performed using a relatively simple set-up. In both tests, the moment and normal force on each cross section can be calculated using equilibrium equations, different to the edge bearing test

[5], which requires solving a hyperstatic problem under the assumption of symmetry for both sides of the ring. This may not be a reasonable approximation for some species like Tre Gai, as documented in a previous study [13]. As expected, no significant differences were found in the outer and inner moduli with both tests.

Important differences with radial position were measured for all the species. Higher failure strains were found at the inner position for EDU, IRI and VIO while no significant differences were obtained for BAM and GA. A lower outer failure strain may be due to the presence of large areas of fiber-matrix interface near the outer boundary due to the higher fiber density. However, the mechanisms of transverse failure of bamboo are complex as found with scanning electron microscope in a recent study [15].

For the European species, a lower stiffness was found for specimens from the higher part of the culm (between 2.5 and 3.5 m from the ground) compared to the stiffness of those from the lower part (between 0.5 and 1.5). This may be attributed to the adaptations of nature during the evolution process since the culms are exposed to the action of the wind, which causes higher shear forces at the lower cross sections.

The mean inner failure strain measured for GA in this study, equal to 0.014, is about 50% higher compared to that obtained with DIC using the edge bearing test, i.e. 0.0092 [18]. The difference may be attributed to the procedure followed to determine strains at the surface. In this study, the strains at the surface were recovered using the assumption that plane sections remain plane after deformation, which was shown to be valid with the finite element verification. The procedure was accomplished since the strains at the surface could not be acquired with DIC due to blurry layers formed parallel to the surface, similar to those seen in the contours presented by Morán et al. [13].

Different to strain, failure strengths are dependent on the adopted constitutive equation. Using the Young's moduli estimated with the linear approximation, the transverse strength at the outer position was generally higher than at the inner, except for Edulis. A recent paper [15] presents second order polynomials fits to the strength measured along the culm wall, normalized with respect to the modulus of rupture of the whole section. Taking into account these results, short calculations yield for that study inner-outer strengths equal to 39.1-23.8 MPa for EDU, and 23.6-25.1 MPa for BAM, which are of the same order of magnitude of the means obtained in this study, i.e. 39.9-14.5 MPa for EDU, and 17.6-30.5 MPa for BAM. The inner-outer mean strengths of 9.9-16.5 MPa obtained for GA are of the same order of magnitude of 6.4-10 MPa obtained with the edge bearing test [18], and 6.1 MPa obtained for the whole cross section with the flat ring test [11].

With respect to the graded elastic modulus, there are few reports to compare with our results. A graded linear model used in a previous study [18] yielded inner- outer moduli

for GA equal to 550-1575 MPa using two specimens. These values have the same order of magnitude of 892-1221 MPa for the inner-outer moduli obtained in this experimental study. The difference may be due to the procedure performed to recover strains at the surface.

In some cases, the coefficients of variation were high, which may be due to the origin of the samples for the European species that combined specimens from the bottom and top parts of the culm. In addition, the number of specimens for the European species was relatively low. This factor may have not allowed determining significant differences, additional to those documented in this study.

4. Conclusions

Two simple protocols, the C and SR tests, can be used to determine the circumferential strain, the tensile strength and the circumferential Young moduli of bamboo at the inner and outer culm wall. The tests are compression based and the specimens can be easily cut from bamboo rings. Similar results for each species were observed from the two tests.

DIC measurements, opportunely modified near the surface of the specimens, allowed measuring the strain profiles.

A closed-form solution that was derived assuming that cross sections remain plane after bending allowed the determination of the graded properties using a simple algebraic procedure.

An effective Young's modulus calculated with the slope of the load-displacement curves was generally between the inner and outer Young moduli obtained with DIC measurements.

The inner failure strain (range of means for all species: 0.014-0.035) was generally higher than the outer (range of means for all species: 0.008-0.0019). VIO and IRI species showed an inner strain 2-3 times significantly larger than the outer.

The effective modulus of GA, i.e. 931 MPa (0.20) and 1148 MPa (0.31) for the SR and C tests, respectively, was lower than those of the European species (range of means for all European species: 1209-2983 MPa).

The inner Young's moduli for all species except EDU (796-1694 MPa) was lower than the outer (range of the means for all species: 1102-4694 MPa). The trend is different for EDU that shows an outer Young's modulus about 30% lower than the inner modulus.

The outer tensile strength of BAM, IRI and GA (range of the means for the three species:16.5-30.5 MPa) was significantly higher than the inner (range of the means for three species: 9.9-17.6 MPa), while no significant differences were found for VIO. A different trend was obtained for EDU, for which the inner strength was about three times higher than the outer.

ACKNOWLEDGMENTS

The author form the University of Bologna wish to thank Roberto Carli and Mario Marcolongo for the technical support during the tests at LISG Lab of the DICAM Department and the students Silvia Greco, Cliff Konrath, Francesco Coppolino and Murat Larcin for their help in performing the tests. J.J. García acknowledges the time given by the Universidad del Valle and the support through a Visiting Professor Fellowship from the Department of Civil, Chemical, Environmental, and Materials Engineering, DICAM of the University of Bologna. The contribution of Richard Morán for the development of the C and SR tests is also acknowledged.

References

[1] https://www.un.org/sustainabledevelopment/sustainable-development-goals/.

[2] K. De Flander, R. Rovers, One laminated bamboo-frame house per hectare per year. Construction and Building Materials 23(1): 210–218, 2009.

[3] J.J.A. Janssen, Designing and Building with Bamboo. Technical Report No. 20, International Network for Bamboo and Rattan, 2000.

[4] P.R. Zea, Percepciones locales versus evidencia científica sobre la relación entre el Bambú y el Agua en el Cantón Bucay Guayas-Ecuador. Universidad de Cuenca-INBAR, 2013.

[5] ISO 22157:2019 Bamboo structures – Determination of physical and mechanical properties of bamboo culms – Test methods. International Organization for Standardization.

[6] L. Villegas, R. Moran, J. Garcia, A new joint to assemble light structures of bamboo slats, Constr. Build. Mater.,98:61–68, 2015.

[7] D. Mitch, K.A. Harries, B. Sharma, Characterization of splitting behavior of bamboo culms, ASCE J. Mater. Civil Eng. 22:1195–1199, 2010.

[8] B. Sharma, K.A. Harries, K. Ghavami, Methods of determining transverse

mechanical properties of full-culm bamboo, J. Constr. Build. Mater. 38:627–637, 2012.

[9] P.H. Lee, M. Odlin, H. Yin, Development of a hollow cylinder test for the elastic modulus distribution and the ultimate strength of bamboo, Construction and Building Materials, 51:235-243, 2014.

[10] L. Torres, K. Ghavami, J. García, A transversely isotropic law for the determination of the circumferential Young´s modulus of bamboo with diametric compression tests, Bahía Blanca: Latin American Applied Research, 2007.

[11] C.A. Rangel, Selección de una teoría de falla para la guadua angustifolia según un modelo de isotropía transversal. Master Thesis. Universidad del Valle, Cali, Colombia, 2012.

[12] J. Virgo, R. Moran, K. Harries, J. García, S. Platt, Flat ring flexure test for full-culm bamboo, 17th International Conference on Non-Conventional Materials and Technologies (17thNOCMAT 2017), Merida, 2017.

[13] R. Moran, K. Weeb, K. Harries, J. García, Edge bearing tests to assess the influence of radial gradation on the transverse behavior of bamboo, *Construction and Building Materials,* 131:574-584, 2017.

[14] J. García, C. Rangel and K. Ghavami, Experiments with rings to determine the anisotropic elastic constants of bamboo, Construction and building of materials, 31:52-57, 2012.

[15] Y. Akinbade, K.A. Harries, C.V. Flower, I. Nettleship, C. Papadopoulos, S. Platt. Through-culm wall mechanical behavior of bamboo. Construction and Building Materials 216:485–495, 2019.

[16] R. Morán, S. Greco, C. Konrath, L. Molari, J.J. Garcia, Experiments with parts of rings to determine the inner and outer circumferential strength of bamboo, NOCMAT 2019, Nairobi, Kenia.

[17] F.B. Beer, E.R. Johnston, Mechanics of Materials, McGraw-Hill, 2007.

[18] R.G. Morán, Desarrollo de juntas con pre-compresión transversal para culmos de Guadua angustifolia Kunth. Ph.D. Thesis. Universidad del Valle, Cali, Colombia, 2019.

Appendix A

If the Young modulus is considered constant along the thickness, the normal stress σ can be calculated as,

$$\sigma = \frac{E\Delta d\varphi}{d\varphi}\frac{(y-e)}{(\rho-y)} \tag{1}$$

The distance *e* and the constant bending stiffness $E\Delta d\varphi/d\varphi$ can be calculated by using static equivalence as the stress distribution is statically equivalent to the bending moment *M and the axial force* N. Thus,

$$\int_A \sigma dA = N \tag{2}$$

$$\int_A \sigma y dA = M \tag{3}$$

By substituing (1) into (2) and(3) and rewrite the equation in terms of a parameter *m*

$$m = \frac{1}{A}\int_A \frac{y}{\rho - y} dA$$

we obtain

$$mA - eA\frac{(1+m)}{\rho} = \frac{N}{E\frac{\Delta d\varphi}{d\varphi}} \tag{4}$$

$$M = -\frac{E\Delta\varphi}{d\varphi} mA(\rho - e) \tag{5}$$

From equation (5) it is possible to obtain the relation for $\frac{E\Delta\varphi}{d\varphi}$

$$\frac{E\Delta\varphi}{d\varphi} = \frac{M}{mA(\rho-e)} \tag{6}$$

Upon replacement of equation (6) into (4) and into (1), the stress distribution and the eccentricity e can be calculated in terms of the bending moment and axial force as,

$$\sigma = \frac{M}{mA}\frac{(y-e)}{(\rho-e)(\rho-y)}, \tag{7}$$

$$e = \frac{m - N/M\rho m}{\frac{1+m}{\rho} - N/Mm} \tag{8}$$

If we assume that the elastic modulus varies linearly across the section of the beam, i.e.

$$E(v) = c_0 + c_1(\rho - y), \tag{9}$$

In terms of the inner and outer radii of the cross section, R_i, and R_o, respectively, and the elastic moduli E_i, E_o at the inner and outer positions of the section, respectively, the elastic modulus

can be written as,

$$E(v) = \frac{E_i R_o - E_o R_i}{R_o - R_i} + \left(\frac{E_o - E_i}{R_o - R_i}\right) v. \tag{10}$$

where $v = \rho - y$.

Substitution of equation (10) into equation (1) yields,

$$\sigma = \frac{\Delta d\phi (c_0 + c_1 v)}{d\phi} \left(\frac{y-e}{v}\right). \tag{11}$$

Considering with expression and the condition of static equivalence (2) and (3):

$$c_0 [mA - \frac{eA}{\rho}(1+m)] + c_1(-eA) = \frac{N}{\frac{\Delta d\phi}{d\phi}}. \tag{12}$$

$$\frac{\Delta d\phi}{d\phi} \int_A (c_0 + c_1 v) \frac{y(y-e)}{\rho - y} dA = M. \tag{13}$$

After some algebra and calling I the inertia moment, we obtain

$$\frac{\Delta d\phi}{d\phi} = \frac{M}{c_0(\rho - e)mA + c_1 I}. \tag{14}$$

Thus, the stress distribution and the eccentricity can be obtained substituting (14) in (11) and and (12).

$$\sigma = \frac{M(c_0 + c_1 v)(y-e)}{[c_0(\rho - e)mA + c_1 I]v} = \frac{M(1 + (\frac{c_1}{c_0})v)(y-e)}{[(\rho - e)mA + (\frac{c_1}{c_0})I]v}. \tag{15}$$

$$e = \frac{\frac{N}{M}(c_0 \rho mA + c_1 I) - c_0 mA}{\frac{N}{M(c_0 mA)} - c_0 \frac{A}{\rho}(1+m) - c_1 A} \tag{16}$$

Appendix B

Castigliano's theorem is applied in both the cases.

For C-shaped:

$$\delta = \frac{dU}{dP} = \frac{d}{dP}\left(\int_0^{\pi} \frac{P^2 R^2 (sen\varphi)^2}{2EI} R d\varphi\right) = \frac{2\pi P R^3}{4EI}$$

$$E = \frac{6\pi R^3}{bt^3} S$$

where U is the internal energy, I the inertia moment I=bt^3/12, S =P/ δ

For Semiring:

$$\delta = \frac{dU}{dP} = \frac{d}{dP}\left(2\int_0^{\pi/2} \frac{P^2(R - Rcos\varphi)^2}{4EI} d\varphi\right) = \frac{2PR^3}{4EI}\left(\frac{3\pi}{4} - 2\right)$$

$$E = \frac{6R^3\left(\frac{3}{4}\pi - 2\right)}{bt^3} S$$